

## Investigation of Properties of Highly Boron-Doped SiGe(C) Thin Layers

Vilius PALENSKIS<sup>1\*</sup>, Romas BAUBINAS<sup>1</sup>, Julius HÅLLSTEDT<sup>2</sup>, Jonas MATUKAS<sup>1</sup>, Henry RADAMSON<sup>2</sup>, Stanislavas SAKALAIUSKAS<sup>1</sup>

<sup>1</sup>Vilnius University, Saulėtekio all. 9, LT-2054 Vilnius, Lithuania;

<sup>2</sup>Royal Institute of Technology (KTH), Electrum 229, Kista-Stockholm, Sweden

Received 02 September 2004; accepted 08 October 2004

A complex study of charge carrier transport, low-frequency noise and surface electric potential distribution of highly boron-doped SiGe(C) layers have been carried out. An attention is paid to the conceptual problem that from Hall-effect measurement for highly degenerated materials we can evaluate the Hall mobility, but for evaluation of mobile charge carrier density one needs to know the effective density of states at the Fermi level energy. The resistivity, Hall coefficient and hole Hall mobility have been measured at temperature range from 77 K to 350 K, while the surface electric potential distribution and the low-frequency noise spectra in the frequency interval from 10 Hz to 20 kHz at room temperature. It is shown that complex investigation of Hall mobility, low-frequency noise and surface electric potential distribution in highly doped SiGe(C) layers gives to one a powerful diagnostic tool for quality characterization of these layers.

**Keywords:** SiGe(C) layers, resistivity, Hall-effect, Hall mobility, drift mobility, highly doped semiconductors, low-frequency noise, surface electric potential.

### INTRODUCTION

SiGe alloy technology offers a great potential for improving novel devices such as high-speed bipolar transistors and metal-oxide-semiconductor devices [1 – 5]. Thin highly doped SiGe layers can be used as the base in n-p-n high-speed bipolar transistors, because SiGe base layer may be thinner and doped to higher dopant concentration level than a normal silicon base. The base resistance is reduced and the frequency performance of the device is improved. There also are some conceptual problems in defining the mobile charge carrier density and its drift mobility in case of highly doped materials [5 – 7].

This study deals with mobile charge carrier transport processes, low-frequency noise characteristics and surface electric potential distributions of boron doped SiGe(C) layers grown on silicon by reduced pressure chemical vapor deposition.

### DETAILS OF INVESTIGATED STRUCTURES AND EXPERIMENTAL SETUP

The SiGe(C) layers used for this study were metastable layers. As the Ge lattice parameter (5.658 Å) is larger than Si (5.431 Å), SiGe layer has compressive strain. The samples were grown on n-type Si (100) substrates (30 – 40 Ω·cm), Ge content in SiGe(C) samples was from 17 % to 28 % with C amount smaller than 0.5 %. Boron doping concentration was in range of  $3 \times 10^{18} - 1 \times 10^{21} \text{ cm}^{-3}$  (Table 1). More information about the SiGe(C) layer formation is presented in [8].

Electrical properties of highly boron-doped SiGe(C) layers strongly depend on germanium, carbon, boron concentration and on defect density. Resistivity, Hall-effect, surface electric potential and low-frequency noise

measurements were performed by using the van der Paw configuration. The resistivity and Hall-effect have been measured at temperatures from 77 K to 350 K. The noise and surface electric potential measurements were performed at room temperature ( $T = 290 \text{ K}$ ). The samples were cleaved in  $10 \times 10 \text{ mm}^2$  or  $15 \times 15 \text{ mm}^2$  pieces and Al contacts were evaporated at corners of each sample. The samples were then annealed for 10 s at  $T = 400 \text{ °C}$ . The concentration of boron doping was determined by using high-resolution X-ray diffraction technique.

**Table 1.** Features of SiGe(C) layers

Sample No.	Layer thickness, nm	Ge content, %	C content, %	Boron doping concentration, $\text{cm}^{-3}$
D-01	34	27.4	–	$1.28 \cdot 10^{19}$
G26-09	120	24	0.45	$3.10 \cdot 10^{18}$
G26-08	127	23	0.39	$6.56 \cdot 10^{19}$
G26-10	160	17.5	0.38	$4.52 \cdot 10^{20}$
B-07	104	22.5	–	$3.73 \cdot 10^{19}$

**Table 2.** SiGe layer characteristics for study of substrate surface etching effect

Sample No.	Ge, %	Boron doping	Layer thickness, nm	Substrate etching
1	21.5	low	83	no
3	21.5	high	83	yes
4	21.5	high	83	no
5	21.5	low	83	yes

There were also carried out a special study of the effect of substrate etching on the above mentioned sample

\*Corresponding author. Tel.: +370-5-2366073; fax: +370-5-2366081.  
E-mail address: vilius.palenskis@ff.vu.lt (V. Palenskis)

characteristics. The investigated in this case sample parameters are represented in Table 2. The low-frequency noise measurement circuit is presented in Fig. 1. Here LNA is the low-noise amplifier and PC is the personal computer. The voltage fluctuations were amplified by the low-noise amplifier, and then the noise spectra at frequencies from 10 Hz to 20 kHz were calculated on the PC using a special input card and the fast Fourier transform algorithm and weighting procedure. The magnitude of the noise spectral density of voltage fluctuations was evaluated by comparison with the thermal noise of standard resistor.

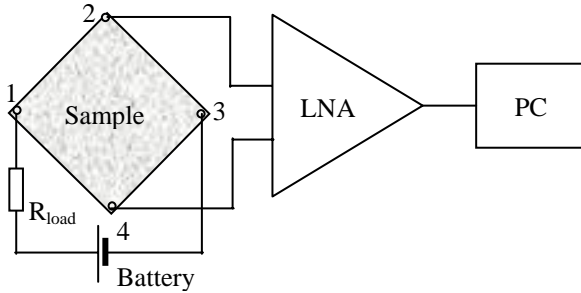


Fig. 1. Noise measurement circuit

The measurement technique for determination of surface electric potential and its distribution is presented in [9].

## INTERPRETATION OF HALL-EFFECT MEASUREMENT RESULTS FOR HIGHLY DOPED MATERIALS

The Hall coefficient by considering the square configuration of the van der Paw sample is defined as [10]:

$$R_H = \frac{U_H d}{IB} F, \quad (1)$$

where  $U_H$  is the Hall voltage,  $d$  is the layer thickness,  $I$  is the direct current (dc), and  $B$  is magnetic flux density (in our case  $B = 0.2$  T), the factor  $F$  is equal to one, which is the case for a perfectly square shaped sample.

Usually from the Hall coefficient data the mobile carrier concentration  $n$  is defined as:

$$n = \frac{r}{qR_H}, \quad (2)$$

where  $r$  is the Hall factor,  $q$  is the free electron charge. But this relation is correct only for nondegenerated semiconductors. In the limit of high magnetic fields or under degenerate conditions, the Hall factor  $r = 1$  [7, 10]. The same statement deals with the conductivity and drift mobility expressions:

$$\sigma = qn \frac{q \langle \tau \rangle}{m^*} \quad (3)$$

and

$$\mu_{dr} = \frac{q \langle \tau \rangle}{m^*}; \quad (4)$$

where  $m^*$  and  $\langle \tau \rangle$  are the effective mass and the averaged relaxation time of mobile charge carriers, respectively. For metals and highly degenerated semiconductors only those charge carriers take place in transfer process, that are in the

vicinity of the Fermi level and the effective mobile carrier concentration  $n_{ef}$  can be expressed as [11, 12]:

$$n_{ef} = N(E_F) kT; \quad (5)$$

where  $N(E_F)$  is the density of states at Fermi level energy  $E = E_F$ ;  $k$  is the Boltzmann constant, and  $T$  is the absolute temperature. This relation is completely confirmed by electronic heat capacity measurements. So, the Hall factor for metals and for all highly degenerated semiconductors  $r = 1$ , and Hall mobility takes the following expression:

$$\mu_H = \frac{q \langle \tau^2 \rangle}{m^* \langle \tau \rangle} = \frac{q \tau_F}{m^*}; \quad (6)$$

where  $\tau_F$  is the charge carrier relaxation time at the Fermi level energy. In many fundamental works for metals and highly degenerated semiconductors it is shown that conductivity is expressed as [11, 12]:

$$\sigma = \frac{1}{3} q^2 N(E_F) v_F^2 \tau_F; \quad (7)$$

where  $v_F$  is the velocity of charge carriers at the Fermi level. In order to define in this case the drift mobility of charge carriers, we must rewrite the conductivity in usual form:

$$\sigma = q n_{eff} \mu_{dr}. \quad (8)$$

From eqs. (5) – (8) one easily obtains the drift mobility expression for highly degenerated semiconductors and metals:

$$\mu_{dr} = \frac{q \tau_F \frac{1}{2} m^* v_F^2}{m^* \frac{3}{2} kT} = \frac{q \tau_F}{m^*} \frac{E_F}{\frac{3}{2} kT} \quad (9)$$

This relation can be written in more general form [7]:

$$\mu_{dr} = \frac{q \langle \tau \rangle}{m^*} \frac{\frac{1}{2} m^* \langle v^2 \rangle}{\frac{3}{2} kT} = \frac{q \langle \tau \rangle}{m^*} \frac{\langle W_k \rangle}{\frac{3}{2} kT}. \quad (10)$$

This expression is also correct for nondegenerated semiconductors because in this case the mean value of kinetic energy of mobile carriers  $\langle W_k \rangle = (3/2) kT$ . The eq. (10) shows that for homogeneous and highly degenerated materials charge carrier drift mobility increases with doping level due to Fermi level energy increase. In order to explain the Hall-effect measurement results of metals and highly doped materials an additional condition must be considered. As shown in [15], for homogeneous metals and highly degenerated semiconductors the charge carrier relaxation time at Fermi level at room temperature is general and equal

$$\tau_F = \hbar / (kT); \quad (11)$$

where  $\hbar = h / (2\pi)$  is the Plank's constant.

The Hall mobility of electrons and holes dependencies on density of single ionized donors  $N_D$  and acceptors  $N_A$  in silicon, respectively, are represented in Fig. 2. The solid lines are approximations of experimental results at temperature  $T = 300$  K [13, 14]. The dashed lines at small concentration of donors  $N_D$  and acceptors  $N_A$  show the Hall mobility components due to lattice scattering, and the dashed lines at high doping levels represent the Hall mobility components due to Heisenberg uncertainty

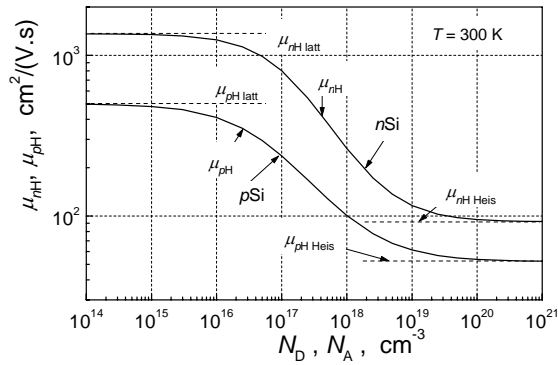


**Fig. 2.** The Hall mobility of electrons and holes dependencies on density of single ionized donors  $N_D$  and acceptors  $N_A$  in silicon, respectively. The solid lines are approximations of experimental results at temperature  $T = 300$  K [13, 14]

principle. For ideal case, when there are no macroscopic faults in the lattice, the hole Hall mobility for high degenerated  $pSi$  at temperature  $T = 300$  K must be about  $50 \text{ cm}^2/(\text{V}\cdot\text{s})$  (it follows from eqs. (6) and (11)). Thus, if Hall mobility is smaller than that value, it unambiguously shows that investigated material or layer has macroscopic defects or material has polycrystalline or amorphous structure, i.e. the mean free path of charge carriers is restricted by various potential barriers.

### EXPERIMENTAL RESULTS OF SiGe(C) LAYERS AND DISCUSSION

The resistivity, Hall coefficient and Hall mobility measurement results of SiGe(C) layers, presented in Table 1, are shown in Figs. 3 – 5, respectively. From these results it is clearly seen, that the resistivity, Hall coefficient and Hall mobility of highly boron-doped SiGe(C) layers have very weak dependency on temperature. For sample D-01 having the layer thickness about 34 nm the observed results were very nonstable. Comparing the obtained experimental Hall mobility results for SiGe(C) layers with that for ideal case (Fig. 2) we can conclude that formed layers have macroscopic defects.

In [16], it is shown that low-frequency noise ( $1/f$ ) level is very sensitive to the material defectiveness. We carried out the noise measurements of these layers. In order to eliminate an influence of contacts, the noise spectra were measured between contacts 2 – 4 (transverse direction),

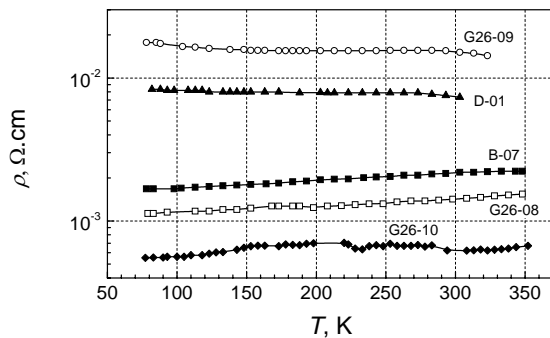


**Fig. 3.** The resistivity of boron-doped SiGe(C) layers, presented in Table 1, dependencies on temperature

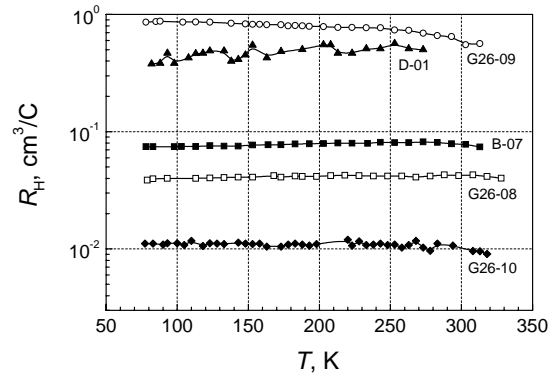


**Fig. 4.** The Hall coefficient of boron-doped SiGe(C) layers, presented in Table 1, dependencies on temperature

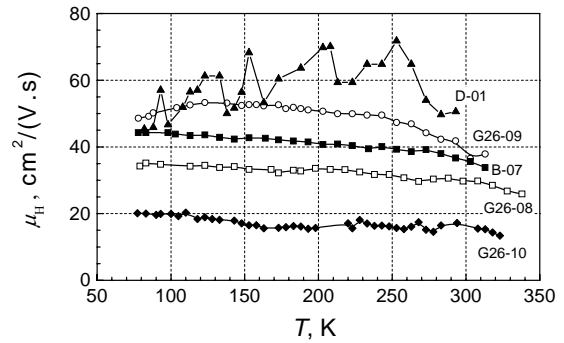


**Fig. 5.** The hole Hall mobility of boron-doped SiGe(C) layers, presented in Table 1, dependencies on temperature

while the direct current was flowing between contacts 1 – 3 (Fig. 1). The obtained relative voltage  $U$  fluctuation spectral density dependencies on frequency for investigated SiGe(C) layers are represented in Fig. 6.

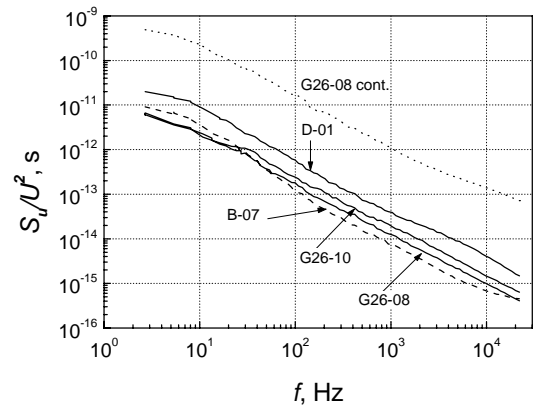


**Fig. 6.** The noise spectra of boron-doped SiGe(C) layers, presented in Table 1. The dot line for sample G26-08 presents the noise spectrum when noise was measured between current flowing contacts 1 – 3 (Fig. 1)

The noise spectra have typical  $1/f$  law which is characteristic for materials having defects. The observed noise level is higher than that for boron-doped silicon [16]. On the other hand, it is also demonstrated that for SiGe(C) layers Al contact interface is not ideal. The obtained results are very useful for further optimization of SiGe(C) layer formation.

## INVESTIGATION OF SUBSTRATE SURFACE ETCHING EFFECT

Here we present the investigation results of SiGe layers (Table 2) formed on substrate *n*-Si (001) after the substrate surface etching in the epitaxy reactor (samples No. 3 and No. 5) and without etching (samples No. 1 and No. 4). The samples No. 1 and No. 5 with low boron doping (about  $6 \cdot 10^{18} \text{ cm}^{-3}$ ) and samples No. 3 and No. 4 having about an order higher boron doping level have been investigated.

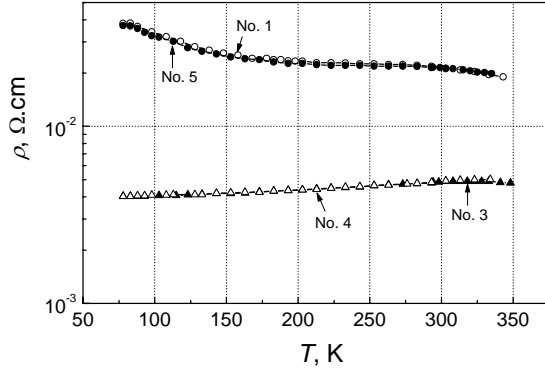


Fig. 7. The resistivity of boron-doped SiGe layers, presented in Table 2, dependencies on temperature

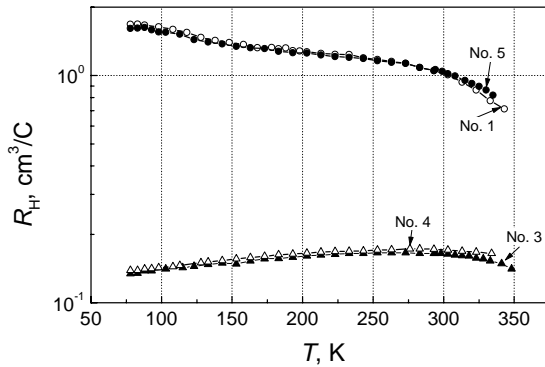


Fig. 8. The Hall coefficient of boron-doped SiGe layers, presented in Table 2, dependencies on temperature

The resistivity, Hall coefficient and hole Hall mobility measurement results in temperature range from 77 K to 350 K are represented in Figs. 7 – 9, respectively. The obtained charge carrier transport characteristics are the same for SiGe layers formed on etched substrate surface or without etching. The hole Hall mobility results at temperature 300 K also are smaller than that for ideal lattice at high doping (Fig. 2).

The low-frequency noise measurement results at various direct current flow directions for samples with low boron doping (sample No. 1) and with high boron doping (sample No. 3) are shown in Figs. 10 and 11, respectively. The relative noise level for sample with higher boron doping (Fig. 11) is about an order lower than one for the sample with low boron doping (Fig. 10). It may be explained in such a way: at higher boron doping, if the

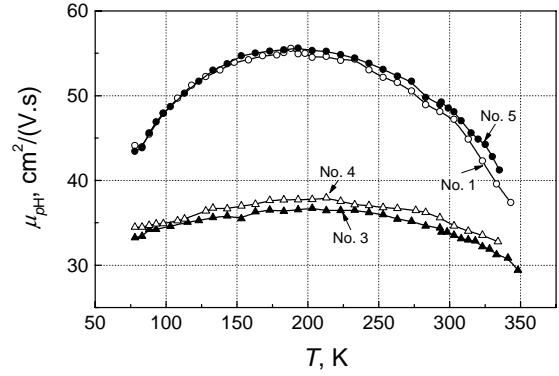


Fig. 9. The hole Hall mobility of boron-doped SiGe layers, presented in Table 2, dependencies on temperature

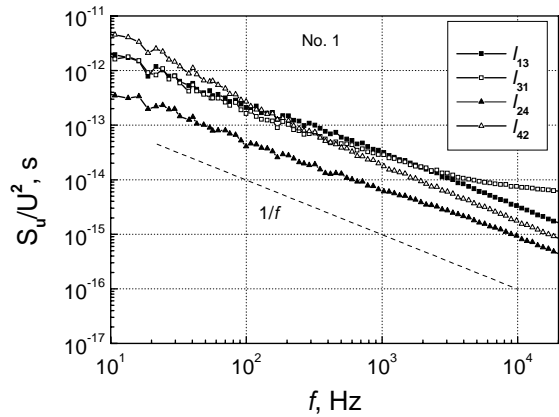


Fig. 10. The noise spectra of SiGe sample No. 1 (with low boron doping) for various directions of current flow (in all cases the noise measurements were performed in transverse direction)

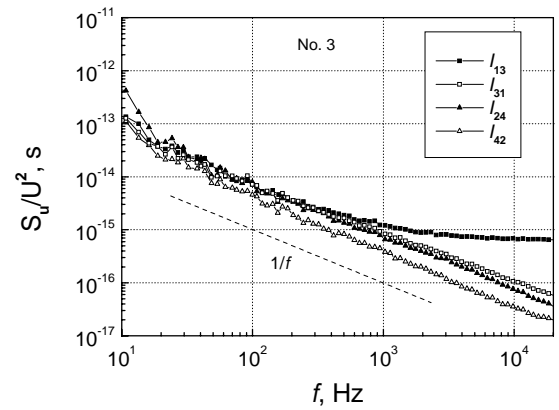
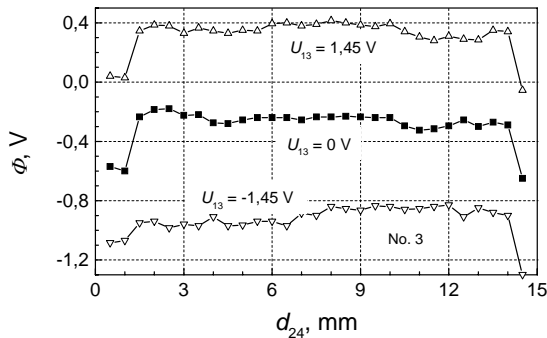


Fig. 11. The noise spectra of SiGe sample No. 3 (with high boron doping) for various directions of current flow (in all cases the noise measurements were performed in transverse direction)

relative number of defects is the same, the noise level is lower for higher doped samples due to more effective screening of defects by mobile charge carriers, i.e. the Debye's screening length is smaller at higher charge carrier density.

## INVESTIGATION OF THE SURFACE ELECTRIC POTENTIAL DISTRIBUTION

In order to get some information on the defect distribution on the area of the SiGe layers we carried out the measurements of the surface electric potential distributions between diagonal contacts of the the sample without applied electric field, and when electric field is applied along the measured diagonal, and when electric field is applied in transverse direction to that diagonal.



**Fig. 12.** The surface electric potential  $\Phi$  distribution along the diagonal 2 – 4, when the bias is applied between transverse diagonal contacts in opposite directions and without applied voltage for sample No. 3 with high boron doping

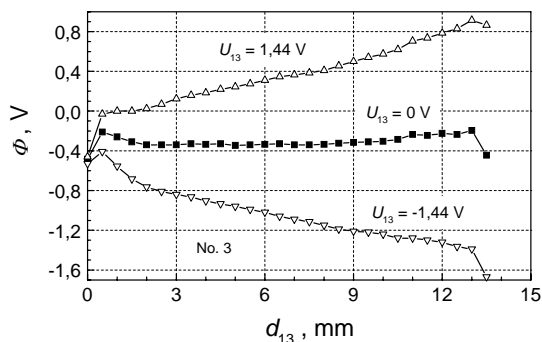


**Fig. 13.** The surface electric potential  $\Phi$  distribution along the diagonal 1 – 3, when the bias is applied along this diagonal in opposite directions and without applied voltage for sample No. 3

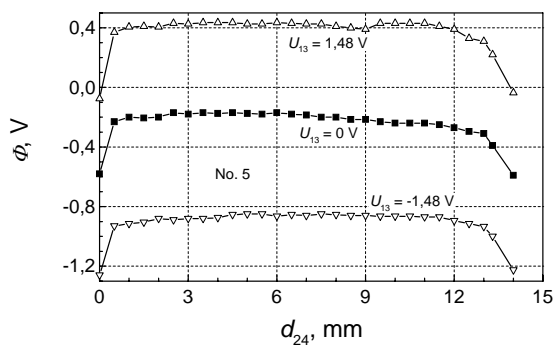


**Fig. 14.** The surface electric potential  $\Phi$  distribution along the diagonal 2 – 4, when the bias is applied between transverse diagonal contacts in opposite directions and without applied voltage for sample No. 5 with low boron doping

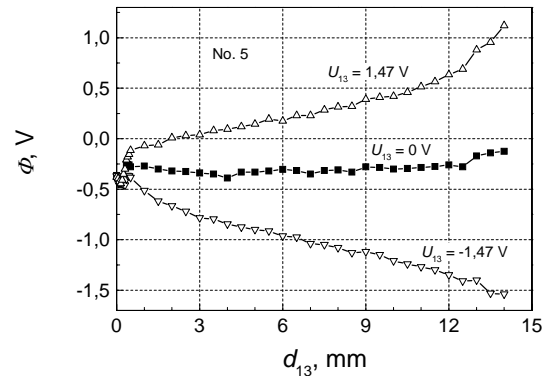


**Fig. 15.** The surface electric potential  $\Phi$  distribution along the diagonal 1 – 3, when the bias is applied along this diagonal in opposite directions and without applied voltage for sample No. 5

The measurement results were calibrated according to the surface electric potential of Au. The surface electric potential  $\Phi$  distribution measurement results along the diagonal, when the bias is applied between transverse diagonal contacts, and when the bias is applied along this diagonal in opposite directions and without applied voltage for sample No. 3 with high boron doping are presented in Figs. 12 and 13. A steep change of the surface electric potential at the beginning and at the end of curves is caused by the transition from Al contact to SiGe layer, i.e. to the different contact potentials of Al film and SiGe layer. From these results we can see some nonhomogeneous distribution of the surface electric potential that may be related with the defects in the SiGe layer and with some pollution of the investigated surface.

The analogical surface electric potential distribution results for SiGe sample with lower boron doping are represented in Figs. 14 and 15. From the measurement results, presented in Figs. 12 and 14, it is seen that surface electric potential distribution is more homogeneous for sample with lower boron doping concentration, i.e. the sample with high boron doping concentration (about  $6 \cdot 10^{19} \text{ cm}^{-3}$ ) has more defects. It can be explained by the fact that boron atom size is larger than one for silicon atom, and the crystal lattice is more damaged at high boron doping concentration. In order to compare the low-frequency noise and the surface electric potential measurement results one must consider that in the case of the surface electric potential we measure the static potential distribution, while the low-frequency noise is caused by fluctuations in time of potential barrier parameters: width and height. The fluctuations of the potential barrier parameters are due to random charge carrier trapping and emission processes by centres localized in these potential barriers. At higher free charge density the fluctuations of the barrier parameters are reduced due to the Debye's screening effect [16].

## CONCLUSIONS

An attention is paid to the fact that from the Hall-effect measurements for highly degenerated materials we can evaluate the Hall mobility, but for evaluation of mobile

charge carrier density one needs to know the effective density of states at the Fermi level energy. It is shown that though SiGe layers with higher boron doping concentration have more defects than ones for lower boron doping, the low-frequency noise level is lower due to the larger Debye's screening effect at higher free charge carrier density. Thus, the complex investigation of Hall mobility, low-frequency noise and surface electric potential distribution in highly doped SiGe(C) layers gives to one a powerful diagnostic tool for quality characterization of these layers.

## REFERENCES

1. **Fobelets, K., Jeamsaksiri, W., Papavasiliou, C., Vilches, A., Gaspari, V., Velazquez-Perez, J. E., Michelakis, K., Hackbarth, T., König, U.** Comparison of Sub-micron Si:SiGe Heterojunction nFETs to Si nMOSFET in Present-day Technologies *Solid-State Electronics* 20 (8) 2004: pp. 1401 – 1406.
2. **Vilches, A., Michelakis, K., Fobelets, K., Haigh, D., Papavasiliou, C., Hackbarth, T., König, U.** Buried-channel SiGe HMODFET Device Potential for Micropower Applications *Solid-State Electronics* 20 (8) 2004: pp. 1423 – 1431.
3. **Isella, G., Chrastina, D., Rösner, B., Hackbarth, T., Hercog, H. J., König, U., Von Känel, H.** Low-energy Plasma-enhanced Chemical Vapor Deposition for Strained Si and Ge Heterostructures and Devices *Solid-State Electronics* 20 (8) 2004: pp. 1317 – 1323.
4. **Kasper, E., Eberhardt, J., Jorke, H., Luy, J.-F., Kibbel, H., Dashiell, M. W., Schmidt, O. G., Stoffel, M.** SiGe Resonance Phase Transistor: Active Transistor Operation Beyond the Frequency  $f_T$  *Solid-State Electronics* 20 (5) 2004: pp. 837 – 840.
5. **Smirnov, S., Kosina, H.** Monte Carlo Modeling of the Electron Mobility in Strained  $\text{Si}_{1-x}\text{Ge}_x$  Layers on Arbitrarily Oriented  $\text{Si}_{1-y}\text{Ge}_y$  Substrates *Solid-State Electronics* 20 (8) 2004: pp. 1325 – 1335.
6. **Fu, Y., Joelsson, K. B., Grahn, K. J., Ni, W.-X., Hansson, G. V., Willander, M.** Hall Factor in Strained  $p$ -type Doped  $\text{Si}_{1-x}\text{Ge}_x$  Alloy *Phys. Rev. B* 54 (16) 1996: pp. 11317 – 11321.
7. **Palenskis, V., Juškevičius, A., Laučius, A.** Mobility of Charge Carriers in Degenerate Materials *Lit. Fiz. Sbornik* 25 (4) 1985: pp. 125 – 132.
8. **Hällstedt, J., Suvar, E., Persson, P. O. Å., Hultman, L., Wang, Y.-B., Radamson, H. H.** Growth of Highly Quality Epitaxial  $\text{Si}_{1-x-y}\text{Ge}_x\text{C}_y$  Layers by Using Chemical Vapor Deposition *Applied Surface Science* 224 2004: pp. 46 – 50.
9. **Sakalauskas, S., Sodeika, A.** Automated Measuring Instrument of the Surface Electric Potential and Potential Distribution *Review of Scientific Instruments* 69 (2) 1998: pp. 466 – 468.
10. **Stillman, G. E., Bose, S. S., Kim, M. H., Lee, B., Low, T. S.** Characterization and Properties of Semiconductors. In: Handbook on Semiconductors, Vol. 3, 2<sup>nd</sup> ed., Elsevier, 1994: pp. 1 – 325.
11. **Ziman, J. M.** Principles of the Theory of Solids. 2<sup>nd</sup> ed., Cambridge: University Press, 1972: 472 p.
12. **Abrikosov, A. A.** Fundamentals of the Theory of Metals. Moscow: Nauka, 1987: 520 p. (in Russian).
13. **Dargys, A., Kundrotas, J.** Handbook on Physical Properties of Ge, Si, GaAs and InP. Vilnius: Science and Encyclopedia Publishers, 1994: 262 p.
14. **Jacoboni, C., Canali, C., Ottaviani, G., Alberigi Quanturana, A.** A Review of Some Charge Transport Properties of Silicon *Solid-State Electronics* 20 (2) 1977: pp. 77 – 89.
15. **Devillers, M. A. C.** Lifetime of Electrons in Metals at Room Temperature *Solid State Commun.* 49 (11) 1984: pp. 1019 – 1022.
16. **Palenskis, V.** Flicker Noise (Review) *Lith. Phys. J.* 30 (2) 1990: pp. 107 – 152.